Theoretical Study of the Dissociation of N_2O in a Transition Metal Ion-Catalyzed Reaction

Ana Martínez,[†] Annick Goursot,*[,‡] Bernard Coq,[‡] and Gérard Delahay[‡]

Instituto de Investigaciones en Materiales, Circuito Exterior s/n, C. U. Apdo. Postal 70-360, C.P. 04510, México, D.F. México, and Laboratoire de Matériaux Catalytiques et Catalyse en Chimie Organique, UMR 5618 CNRS; ENSCM, 8 rue de l'Ecole Normale, 34296 Montpellier, Cédex 5, France

Received: December 11, 2003

Models of Fe−zeolites have been used to study the dissociation of N_2O, with and without the presence of ammonia. From Density Functional Theory calculations, the mechanism and energetics of N_2O decomposition paths are presented and discussed. The influence of ammonia is analyzed. The results obtained for a single metal ion and for models including a zeolite cluster are compared. The approximate activation barrier calculated with this cluster model is in good agreement with experiment. The presence of two ammonia ligands reduces the calculated activation barrier, leading to the conclusion that ammonia plays a role in both steps of the N_2O decomposition, i.e., the breaking of the ON_2 bond and the reduction of the iron-oxo compounds.

1. Introduction

Nitrous oxide has been identified as an ozone-depleting agent and as a greenhouse gas. At present, the N_2O concentration is rising by 0.25% in the atmosphere, every year, and the main causes for this increase are the anthropogenic activities. N_2O emissions from industrial processes can be the most easily controlled. Off-gases from adipic acid plants contain N_2O in high concentration, which can be either catalytically decomposed, by the highly exothermic reaction[1] $N_2O \rightarrow N_2 + {}^1/_2O_2$ ($\Delta H^\circ = -39$ kcal mol^{-1}), or valorized in the low temperature oxidation of methane and benzene using very efficient Fe−zeolite catalysts, independently discovered in 1988.[2] It was proposed that N_2O interaction with Fe−ZSM-5 yields a very active surface oxygen, commonly called α-oxygen.[3] From both experimental and theoretical studies, this species was proposed to be associated with Fe in binuclear[4−6] or mononuclear[7] oxo-cations.

When N_2O is present at very low concentration in tail-gas from nitric acid plants and power plants, the simplest control technology for N_2O removal would also be based on the catalytic decomposition, and Fe−zeolites are among the most active materials in the presence of O_2, although they remain somewhat inefficient. However, a boosting effect on the N_2O decomposition was experimentally identified when adding a hydrocarbon, CO or NH_3, on Fe−ZSM-5, Fe−ferrierite (Fe−FER) and Fe−zeolite beta (Fe−BEA) catalysts.[8] From experimental results,[8f] the reduction of N_2O by NH_3 is regulated by the redox cycle $Fe^{II} \Leftrightarrow Fe^{III}$. In the first step, N_2O formally oxidizes Fe^{II} in Fe^{III} with formation of N_2 according to

$$Fe^{II} + N_2O \rightarrow \text{“}Fe^{III}O\text{”} + N_2$$

In the second step, NH_3 removes the adsorbed oxygen leading back to the Fe^{II} species

$$\text{“}Fe^{III}O\text{”} + 2/3\ NH_3 \rightarrow Fe^{II} + 1/3\ N_2 + H_2O$$

Upon the interaction of N_2O with Fe−BEA, different surface oxygens O* would exist associated with one or two Fe atoms, the former being the most reactive oxo-cation species with respect to H_2 or CO.[9] The role of the reductant in the catalytic decomposition of N_2O is not fully understood: it may facilitate the removal of surface oxygens O*, but also take part directly to the $O-N_2$ dissociation reaction. Recent theoretical studies have investigated the decomposition of N_2O over Fe−zeolites, without reductant. Yakovlev et al.[10] have used $Fe(OH)_3(H_2O)_2$ to model the metal site, studying the decomposition mechanism. Another study showed that oxo metal cations could also be possible active sites for N_2O decomposition.[11] Very recently, Ryder et al.[12] have analyzed the further steps of N_2O decomposition, starting from the zeolite−FeO compound. However, several aspects of the reaction still remain unclear, particularly the role of the zeolite framework and the effect of NH_3.

To achieve a better understanding of the decomposition of N_2O on Fe−zeolites mediated by ammonia, we have used density functional theory (DFT) calculations to analyze the effect of the zeolite framework in the interaction of N_2O with the Fe(II) extraframework cations and to verify if this interaction is modified by the presence of NH_3. We chose to consider zeolite beta (BEA) as a model, because Fe−BEA was proven very efficient for the N_2O decomposition, helped or not by the presence of NH_3.[8e,f]

We compare then our results concerning the energetic of N_2O in Fe−BEA with recent experiments obtained in our laboratory, i.e., the adsorption enthalpy of N_2O at 300 K and the apparent activation energy for N_2O decomposition at 500 K. The very good agreement between calculated and experimental values allows us to validate our methodology, in particular, for the reaction in the presence of NH_3, for which it is not experimentally possible to estimate the activation barrier to N_2O decomposition.

2. Models

BEA has a widely open three-dimensional channel structure, with 12-membered ring apertures, leading to a full accessibility of the extraframework cations.[13] Substitution of Si by Al induces a negative charge in the framework, which has to be compensated by the presence of a counterion. The distribution of Al in the framework, generated during the synthesis in the presence

* To whom correspondence should be addressed. E-mail: goursot@rhodium.enscm.fr.

[†] Instituto de Investigaciones en Materiales.

[‡] Laboratoire de Matériaux Catalytiques et Catalyze en Chimie Organique.

10.1021/jp0313167 CCC: $27.50
Published on Web 05/27/2004

of triethylammonium template, remains unknown, although the Si/Al ratio is controlled. The structure of transition metal ion (TMI) sites is determined by both local and non local criteria. The coordination of TMI to the framework is mainly a local factor. However, the relative positions of other (Al, cation) couples also influence the geometry of TMI sites and are more related to non local effects. To generate a reasonably realistic model cluster, a dozen of periodic solid models were analyzed, after substituting aluminum for silicon atoms, with a Si/Al ratio of 13 and random Al distributions obeying the Löwenstein rule.[14] The structures of these solids were then optimized using a standard force field for zeolites.[15] The Fe cations located in the main channels of BEA were all found to be coordinated to 3(4) oxygens belonging to 4m-, 5m-, and 6m-rings. This coordination to framework oxygens with 4 short, or 3 short and one longer bonds, is in agreement with recent quantum mechanics calculations on various TMI-zeolite systems,[16−18] and this could be a common local factor between TMI sites in different zeolitic structures. Since all solids with different Al distributions were leading to comparable Fe(II) sites, we have selected one model where Fe(II) was located in the main channel and was compensating the charges of two Al separated by only one Si, allowing to cut a reasonably small cluster. This cluster corresponds to a minimum structure, which is sufficient to reproduce the properties of a TMI-zeolite site, as already shown in a previous work on Cu(II)-zeolite models of various sizes.[19,20] This cluster, terminated with H atoms, is presented in Figure 1a. The terminal O−H bonds have been set to 0.96 Å. To preserve the original structure of the zeolite, the H atoms have been positioned along the corresponding Si−O bonds. The geometry has then been optimized, keeping the terminal H fixed in order to simulate the constraints of the remaining solid, assumed to be rigid.

3. Methods

Previous and present results show that divalent TMIs in zeolites receive a substantial amount of electron density from the framework.[17,19] Even if the calculated amount of this charge redistribution depends on the methodology used (exchange-correlation functional, population analysis), the zeolite structure and the nature of the TMI, one can estimate that the formal +2 metal charge is reduced to +0.7−1.3.[17,19] This led us to compare the reaction of N_2O with the Fe−BEA cluster and with a single Fe^+ cation. It should be noted that this crude approximation for the iron site also implies the constrain of a fixed Fe configuration ^6D (d^6s, Fe^+), whereas the presence of the zeolite ligand lowers the spherical symmetry of the TMI and allows a fractional occupation of the metal orbitals.

The reaction we have studied can be schematized as

$$\underset{\text{reactants}}{\text{model} + \text{O}{-}\text{N}_2} \leftrightarrow \underset{\text{adsorption complex}}{[\text{model}{-}\text{ON}_2]} \leftrightarrow \underset{\text{transition state (TS}^{\#})}{[\text{model}{-}\text{O}{-}\text{N}_2]^{\#}} \rightarrow \underset{\text{products}}{\text{model-O} + \text{N}_2} \quad (1)$$

We have compared the energetic of reaction 1 when the catalytic site (model) is represented by the cluster Fe−BEA (Figure 1a) or a single Fe^+ cation. The presence of NH_3 has then been studied using the cluster Fe−BEA including two NH_3 molecules compared with $[Fe(NH_3)_2]^+$. Figures 2−6 illustrate this reaction for the different models, as described in section 4.

3.1. Computational Details. The calculations have been performed within the Linear Combination of Gaussian-Type Orbitals-Density Functional formalism (LCGTO-DF) using the deMon programs[21,22] and the Gaussian 94[23] code.

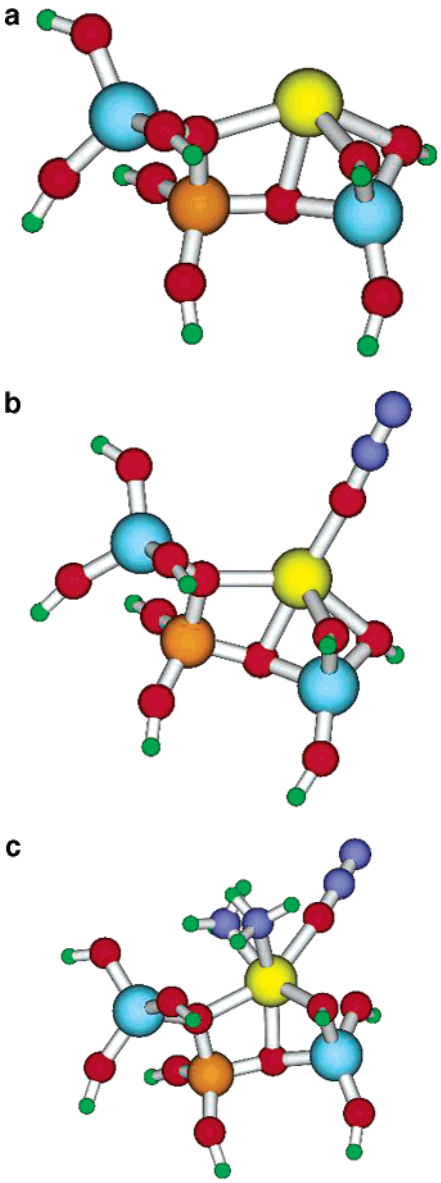

Figure 1. Optimized structures of the clusters representing Fe−BEA (a), N_2O−Fe−BEA (b) and N_2O−Fe−BEA$(NH_3)_2$ (c); Fe is tetracoordinated to 4 zeolite-oxygens.

The geometries of the BEA models have been optimized at the nonlocal level of theory using gradient-corrected (GGA) functionals (Perdew and Wang[24] functional for exchange and Perdew[25] for correlation). The bases used for the BEA cluster were of DZVP quality[26] for Si/Al (6321/521/1*), O/N (621/41/1*), and H (41/1), whereas two bases of TZ[27] and QZ[28] quality were compared for Fe. The auxiliary function sets[26] used to fit the charge density and the exchange-correlation potential were (5,5;5,5) for Fe, (5,2;5,2) for O/N, (5,4;5,4) for Si/Al and (5,1;5,1) for H.

For the study of reaction 1 with Fe^+, the calculations have been performed with the Perdew and Wang[24] or the Becke[29] functional for exchange, whereas the Perdew[25] functional was used for correlation.

It is well-known that a good description of the term energies of TM atoms is very difficult, due to both theoretical and methodological errors. DFT includes a good treatment of electron correlation, but fails in many cases to reproduce degenerate energies for degenerate orbitals and redundancy relations.[30−33] Moreover, several determinants are often necessary to estimate multiplet energies. However, as indicated by

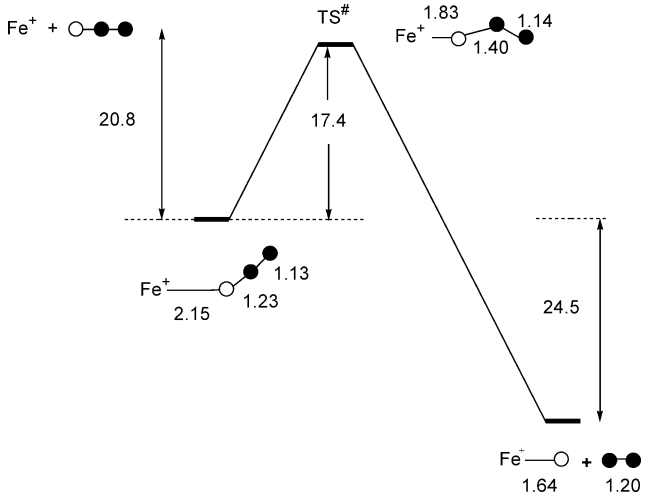

Figure 2. Scheme of the reaction of Fe^+ with $O-N_2$, including the calculated transition state TS#. (Energy differences ΔU ($T = 0$ K) in kcal mol^{-1};white and black balls represent oxygen and nitrogen atoms, respectively.)

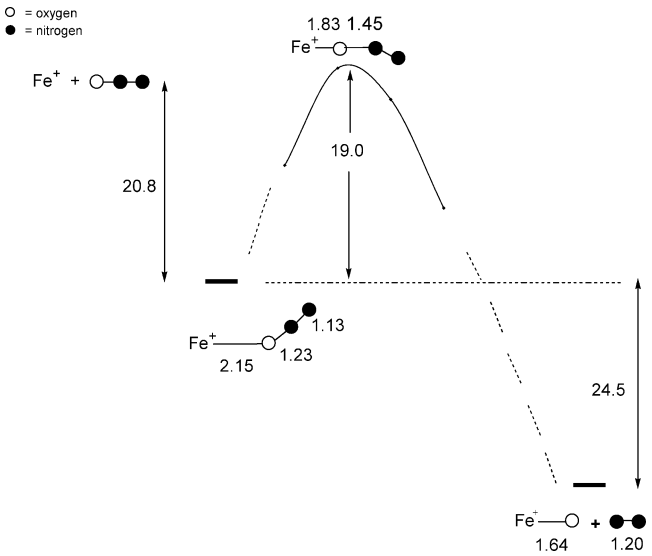

Figure 3. Scheme of the reaction of Fe^+ with $O-N_2$, with an approximate reaction path for the $O-N_2$ dissociation (see text). (Energy differences ΔU ($T = 0$ K) in kcal mol^{-1}; white and black balls represent oxygen and nitrogen atoms, respectively)

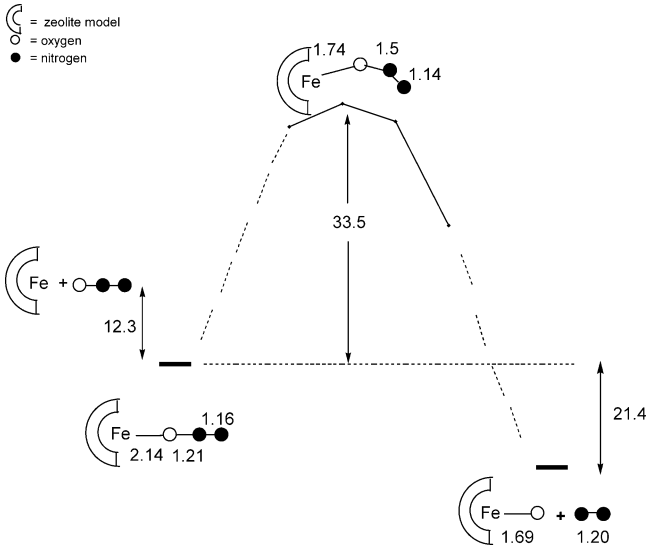

Figure 4. Scheme of the reaction of Fe−BEA with $O-N_2$, with an approximate reaction path for the $O-N_2$ dissociation (see text). (Energy differences ΔU ($T = 0$ K) in kcal mol^{-1}; white and black balls represent oxygen and nitrogen atoms, respectively.)

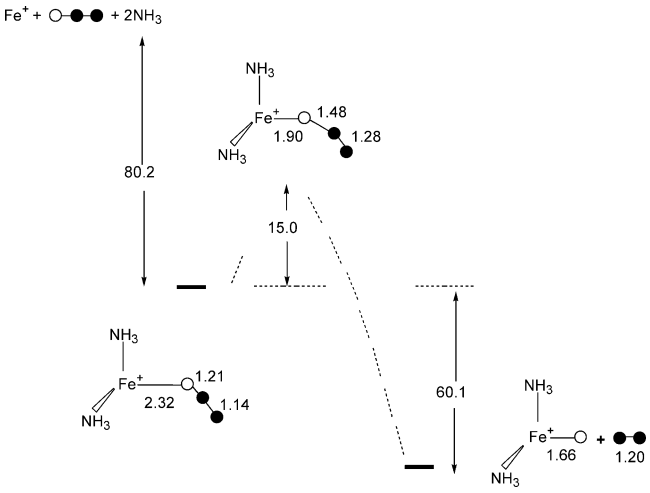

Figure 5. Scheme of the reaction of Fe^+ with $O-N_2$ and 2 NH_3, with an approximate reaction path for the $O-N_2$ dissociation (see text). (Energy differences ΔU ($T = 0$ K) in kcal mol^{-1}; white and black balls represent oxygen and nitrogen atoms, respectively.)

the diagonal-sum rule,[34] one can always calculate, as a single determinant, the ground-state of a given configuration, using the max M_L and M_S values. This procedure, associated with a good description of the degeneracy of the 3d orbitals,[31,35] leads to quite reasonable results by comparison with experiment,[36] given a good choice of orbital basis sets, which become critical parameters when the relative energies of $d^n s^2$ and $d^{n+1}s^1$ configurations are concerned. Since we are mainly dealing with an Fe^+ electron structure in Fe−BEA, the Fe basis must be chosen so as to reproduce correctly the energy difference between the ground-states of the $3d^6 4s^1$ (^{6}D) and $3d^7$ (^{4}F) Fe^+ configurations, which will be involved in binding adsorbents. Table 1 compares the results obtained for various orbital bases and two exchange-correlation functionals. Whereas Fe presents a severe difficulty for most of the commonly used bases, the values obtained for Fe^+ remain generally reasonable, especially for the bases (2), (3), and (4).

Basis (3) has been used in the study involving the isolated Fe^+ cation, associated with 6311-G+[27] bases for the other atoms. Basis (4) for Fe, associated with DZVP bases[26] for the other atoms, has been used for the calculations involving the BEA model, as in previous studies on Cu(II)-zeolites.[16,40]

Models including the single cation Fe^+ have sextet ground-states, whereas those including BEA−Fe have quintet ground-states.

3.2. Energetic of the Reaction. The electronic energies calculated from DFT have been corrected for the zero point level, assuming the harmonic oscillator approximation. The corresponding differences in standard internal energy ΔU^0 at $T = 0$ K are presented in the Figures.

As proposed by Trout et al.,[41] we have used only the vibrational frequencies of the Fe−adsorbate species in the evaluation of the vibrational contributions to $\Delta U°$, assuming that the presence of the adsorbed molecules does not modify significantly the Fe−BEA vibrations. For the gaseous molecules, the translational, rotational, and vibrational contributions have been taken into account.

Standard enthalpy differences are calculated using the expression $\Delta H° = \Delta U^0 + \Delta n\ RT$, all zeolite compounds being assumed to be incompressible and all gases ideal, where Δn

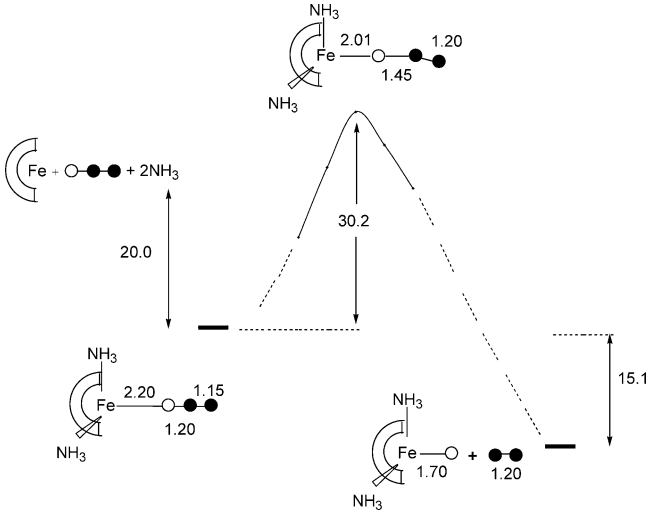

Figure 6. Scheme of the reaction of Fe−BEA with $O-N_2$ and 2 NH_3, with an approximate reaction path for the $O-N_2$ dissociation (see text). (Energy differences ΔU ($T = 0$ K) in kcal mol^{-1};white and black balls represent oxygen and nitrogen atoms, respectively.)

TABLE 1: Energy Difference (eV) between the ^6D ($3d^6 4s^1$) (taken as origin) and the ^4F ($3d^7$) States of Fe^+, Calculated with Different Bases and Functionals and Compared with Experimental Value

basis	Becke[29]−Perdew[25] functionals	Perdew[24]−Perdew[25] functionals
(1) DZ[26]	−0.38	−0.12
(2) TZ[26]	0.09	0.17
(3) TZ (6311-G$^+$)[27]	0.19	0.26
(4) QZ (Wachters)[28]	0.19	0.08
(5) TZ[37]	0.58	0.70
(6) DZ-ANO[38]	0.28	0.47
experimental value[39]	0.25	

represents the difference in moles between the products and the reactants in the chosen equilibrated reaction.

The Eyring equation, based on the "transition state" model, or "activated complex" method has been extended to surface reactions and is used in heterogeneous catalysis to estimate reaction rates.[42−44] Combining the Arrhenius equation with the Eyring equation allows one to evaluate thermodynamic parameters which can be measured experimentally, especially the apparent activation energy E_a of N_2O decomposition (at ca. 500 K), related to the reaction rate of oxidation of Fe^{II}-BEA by N_2O (experimental rate $= k_0 \exp(-E_a/RT)$). The true activation energy (from the adsorption complex to the transition state) encompasses two terms and it is obtained after adding the appropriate heat of adsorption (formation of adsorption complex from the reactants) to the apparent activation energy. However, we will focus essentially on the apparent activation energy, since it is the property which can be measured experimentally.

The "activated complex" method pictures the direct reaction between reactants proceeding through an activated complex, or transition state $TS^{\#}$, that, later, breaks further into products.

Using the Eyring equation and the formal expression of the apparent activation energy leads to the expression of the rate constant of the equilibrated reaction to the activated complex: $k = k_0 \exp(-E_a/RT)$, with $k_0 = B \cdot \exp(-2) \cdot \exp(\Delta S^{\#}/RT)$ and $B = k_B T/h$, where k_B, h, R are the Boltzmann, Planck and rare gas constants, respectively, and $T = 500$ K.

The apparent activation energy is calculated using $E_a = \Delta H_a^{\#} + 2RT$, where $\Delta H_a^{\#}$ is the apparent enthalpy of activation, i.e., the difference between the transition state and reactant enthalpies. $\Delta H_a^{\#}$ is evaluated as $\Delta U_a^{\#} + RT$, with $\Delta U_a^{\#}$ being the difference in internal energies between the activated complex and the reactants at the experimental $T = 500$ K.

TABLE 2: Atomic Electron Distribution in the Models without NH_3, Estimated Using the Mulliken Population Analysis and Mayer BO[47] Values; Fe Spin Density (σ) Is Also Indicated

	Mulliken net charges			Mayer BO	
	Fe (σ)	zeolite framework	ON_2	Fe−ON_2	O−N_2
Fe^+	+1.0 (*5.0*) ($s^{1.0}$ d^6)				
$[Fe-ON_2]^+$	+0.93 (*4.80*) ($s^{0.66}$ $d^{6.41}$)		+0.07	0.13	1.42
$[Fe-ON_2]^+$ ($O-N_2 = 1.39$ Å, TS)	+1.05 (*4.65*) ($s^{0.49}$ $d^{6.46}$)		−0.04	0.67	0.96
Fe−BEA	+1.05 (*3.60*) ($sp^{0.28}d^{6.67}$)	−1.05			
N_2O−Fe−BEA	+1.15 (*3.60*) ($sp^{0.27}$ $d^{6.58}$)	−1.20	+0.04	0.17	1.54
N_2O−Fe−BEA ($O-N_2 = 1.50$ Å, approximate TS)	+1.19 (*3.65*) ($sp^{0.27}$ $d^{6.54}$)	−0.98	−0.21	0.93	0.78

The apparent entropy of activation, which is negative because two species associate to form only one, enters into the pre-exponential factor k_0, i.e., in the kinetics of the decomposition.

4. Results and Discussion

The full path including the transition state search has been performed for $[Fe-ON_2]^+$, to validate the search for an approximate $O-N_2$ dissociation path, which is a reasonably accurate and low-cost way of locating possible intermediates in the reaction. This methodology has been applied with great success in many problems involving the analysis of a complex potential energy surface for different reactions.[45]

4.1. Adsorption of N_2O. The interaction between the zeolite framework model and the Fe(II) cation (Figure 1a) generates a substantial redistribution of electron density, since the calculated Mulliken net charge of Fe is +1.05 instead of +2 (Table 2). In parallel, the Fe spin density (σ) is reduced from 4.0 (isolated Fe^{2+}) to 3.6 in BEA−Fe. Charge and spin redistributions have also been reported for a Cu−Y zeolite and the estimated spin delocalization was supported by the comparison between theoretical and experimental hyperfine coupling constants.[16,20] It is worth noting that, as expected, admixture of the Hartree−Fock exchange in the B3LYP functional leads to weaker metal−ligand interactions and to a larger localization of the spin density on the TMI, as compared to a pure GGA exchange and correlation functional. This result is consistent with the Fe spin density of 3.78 calculated for Fe(II)-ZSM-5, in a recent work based on B3LYP calculations.[46]

Binding N_2O to the BEA model leads to a complex illustrated in Figure 1b. The Fe−O bond is 2.136 Å long, whereas the N−O (1.209 Å) and N−N (1.156 Å) bond lengths are comparable with those calculated for the isolated N_2O molecule (1.211 and 1.154 Å, respectively). The bonded Fe−ON_2 group remains close to linear. If one neglects the role of the framework in the interaction with N_2O, one can say that the [zeolite(−2) Fe(+2)] site behaves as an Fe^+ cation. This is certainly an oversimplification but it can be helpful in a first step, to reach a better understanding of the role of the BEA framework in the reaction.

Binding N_2O to Fe−BEA does not induce a dramatic change in the electron distribution of Fe−BEA (Table 2). There is a slight loss of iron electronic charge upon ligand addition, to the benefit of the BEA cluster, with no change of the spin density distribution. The TMI configuration remains intermediate

between the $4s^13d^6$ and $3d^7$ Fe^+ configurations, which are very close in energy for the isolated cation (Table 1). The presence of the zeolite cluster allows the participation of the 4p orbitals. In fact, the calculated electron distribution of $[Fe-ON_2]^+$ shows that the adsorption of one ligand promotes electronic charge from the 4s into the 3d Fe orbitals.

Binding N_2O to Fe^+ leads to the complex $[Fe-ON_2]^+$, 20.8 kcal $mole^{-1}$ more stable than the reactants (Figures 2 and 3). This stabilization is larger than the one calculated in the Fe−BEA cluster, 12.3 kcal $mole^{-1}$ (Figure 4). In both cases, the $Fe-ON_2$ Mayer bond order (BO),[47] taken as a measure of the bond strength is weak and the O−NN BO at 1.4−1.5 is decreased with respect to the value of 1.75 obtained in the isolated N_2O molecule. The decreased metal−ligand adsorption energy in the presence of a zeolite cluster with respect to the isolated cation is due to short-range interactions between the metal−ON_2 part and the zeolite model. It has been pointed out for other models of zeolites that the decrease in binding energy is very little sensitive to the size of the model cluster.[48] The structures of the $Fe-ON_2$ group in both Fe^+ (Figure 2) and Fe−BEA (Figure 4) models are very comparable, except the bent structure (⟨Fe−O−N_2⟩ bond angle of 137°, instead of 176° in the Fe−BEA model). This is however not a determinant fact, since the stabilization with respect to a linear structure is less than 1 kcal $mole^{-1}$.

As illustrated in Figure 2, the transition state ($TS^{\#}$) to O−NN dissociation of the simple model $[Fe-ON_2]^+$ is 17.4 kcal mol^{-1} higher in energy than the initial complex. This transition state presents a negative frequency at -601 cm^{-1} corresponding to the mode of vibration for the dissociation of the O−N bond. The Fe−O bond length at the transition state (1.83 Å) is shorter than for the stable complex, while the N−O bond distance is much longer (1.40 Å). The complex is no more linear, with a ⟨Fe−O−N⟩ bond angle of 167° and a ⟨O−N−N⟩ bond angle of 144°. The transition state structures of $[Fe-ON_2]^+$ and $Fe-ON_2$ are different, due to the smaller binding energy of ON_2 to Fe in the neutral complex, which involves a longer Fe−O bond (2.08 Å) and a shorter $O-N_2$ bond (1.26 Å) in this neutral species.[49]

The reaction products are $[Fe-O]^+$ and N_2, with a stabilization energy of 24.5 kcal $mole^{-1}$ with respect to the initial complex. Going from the minimum to the transition state, the Fe ion has transferred some charge (0.11 el.) and some spin density to the distorted molecule.

The approximate reaction path search has been performed point by point on the potential energy surface, fixing the N−O bond elongation as the reaction coordinate and relaxing all other coordinates. This procedure will thus overestimate the true activation barrier. To test this procedure, we show in Figure 3 the results obtained for $[Fe-ON_2]^+$. Each N−O bond distance fixed corresponds to one point on the curve. This approximate dissociation path is reaching a maximum 19.0 kcal mol^{-1} higher in energy than the original complex (Figure 2). The main geometrical differences between this species of maximum energy and the calculated $TS^{\#}$ are the O−N bond, which is 0.05 Å longer at the maximum and the ⟨Fe O N N⟩ dihedral angle equal to 60° instead of 180°. Assuming that this approximation is quite reasonable, we have adopted a similar search for all other models.

The approximate dissociation path for $BEA-Fe-ON_2$ is presented in Figure 4. The maximum energy point is 33.5 kcal mol^{-1} higher than the adsorption complex and thus 21.2 kcal mol^{-1} higher than the reactants. The O−N bond is elongated to 1.50 Å and the Fe−O bond is strongly decreased to 1.74 Å.

TABLE 3: Specific Activity in TOF (s^{-1}) and Apparent Activation Energy for the N_2O Dissociation in Two Fe−BEA Catalysts (data adapted from ref 49)

0.40 wt %Fe−BEA		1.9 wt %Fe−BEA	
T/K	TOF /$s^{-1} \times 10^3$	T/K	TOF /$s^{-1} \times 10^3$
486	0.15	460	0.018
490	0.16	467	0.025
493	0.21	475	0.032
496	0.24	482	0.040
500	0.29	490	0.049
503	0.32	497	0.069
507	0.37	505	0.094
510	0.43	512	0.123
513	0.48	520	0.156
		528	0.20
E_a/kcal mol^{-1}	21.4		19.7

Moreover, there is a greater modification in the electron charge distribution than in the case of $[Fe-ON_2]^+$, with more electronic charge transferred to the ON_2 part, coming essentially from the BEA cluster. This is confirmed by the fact that the Fe spin density remains unchanged ($\sigma = 3.60$)

A common feature between the $TS^{\#}$ and the points at the maximum of the approximate path is that their structures display shortened Fe−O bonds associated with elongated O−N bonds. This concerted effect is illustrated by the changes in the Mayer BOs, which show an increase of the Fe−O BO value by a factor of about 5, whereas the O−N BO value decreases by a factor of 1.5 or 2 (Table 2). Actually, this concerted metal−O bond strengthening with $O-N_2$ bond weakening going from the initial complex to the transition state structure is reasonable, leading to short Fe−O bonds in the final product (1.6−1.7 Å). A similar effect has been also shown in previous B3LYP studies of $[Fe-ON_2]^+$ (Fe−O shortened by 0.4 Å, $O-N_2$ lengthened by 0.27 Å)[50] and $^3[Cu-ON_2]^+$ (Cu−O shortened by 0.2 Å, $O-N_2$ lengthened by 0.1 Å).[51]

It is of interest to compare the activation barrier from the reactants, $BEA-Fe + N_2O$, to the approximate transition state, $BEA-Fe-O-N_2$, with the apparent activation energy determined experimentally for N_2O dissociation on Fe-based catalyst. This comparison can be made with data derived from the N_2O dissociation, actually the N_2 evolution, performed on two Fe−BEA catalysts composed of cationic Fe species.[52] Table 3 presents the specific activities (in TOF, number of N_2O molecules dissociated per Fe atom and per second) and the calculated apparent activation energies ($TOF = k_0\exp(-E_a/RT)$). The experimental values of the apparent activation energy E_a are 19.7 and 21.4 kcal mol^{-1}. The apparent activation energy, calculated at 500 K, using the activated complex theory (see section 3.2), leads to a value of $E_a = 22.9$ kcal mol^{-1}, in good agreement with the experimental values.

It is worth noting that such a calculation performed on the basis of reaction 1 modeled with Fe^+ (Figure 2 or 3), instead of Fe−BEA, leads to an activation energy close to zero, which is in disagreement with experiment.

The enthalpy $\Delta H°$ at 300 K for N_2O adsorption:

$$Fe-BEA \leftrightarrow [Fe-BEA-ON_2]$$

has been calculated as -13.4 kcal mol^{-1}, whereas the experimental measurement at the same temperature on an Fe−BEA catalyst leads to the value of 13.2 kcal mol^{-1}.[53] The adsorption enthalpy for $Fe^+ + N_2O$, i.e., -22 kcal mol^{-1}, is much larger as compared to the experimental value found on Fe−BEA.

These results show that the energetic of both N_2O chemisorption and activation is properly described with the model

TABLE 4: Atomic Electron Distribution in the Models with NH_3, Estimated Using the Mulliken Population Analysis and Mayer BO[47] Values; Fe Spin Density (σ) Is Also Indicated

	Mulliken net charges				Mayer BO		
models	Fe (*s*)	zeolite framework	ON_2	$(NH_3)_2$	$Fe-ON_2$	$O-N_2$	Fe−N
Fe^+	+1.0 (*5.0*) ($s^{1.0}$ d^6)						
$[(NH_3)_2Fe-ON_2]^+$	+0.70 (*4.85*) ($s^{0.88}$ $d^{6.42}$)		0.00	+0.30	0.08	1.43	0.17
$[(NH_3)_2Fe-ON_2]^+$ (O−N_2 = 1.48Å, approximate TS#)	+0.85 (*4.60*) ($s^{0.70}$ $d^{6.45}$)		−0.13	+0.28	0.70	0.79	0.20 0.20
Fe−BEA	+1.05 (*3.60*) ($sp^{0.28}d^{6.67}$)	−1.05					
$N_2O-Fe(NH_3)_2-BEA$	+1.19 (*3.70*) ($sp^{0.37}$ $d^{6.42}$)	−1.45	−0.03	+0.29	0.12	1.60	0.43 0.26
$N_2O-Fe(NH_3)_2-BEA$ (O−N_2 = 1.45Å, approximate TS#)	+1.32 (*3.65*) ($sp^{0.36}$ $d^{6.30}$)	−1.37	−0.33	+0.38	0.42	1.04	0.48 0.29

Fe−BEA, whereas it is not if the catalytic site is reduced to a single iron cation.

4.2. Adsorption of N_2O and NH_3. According to experimental results, between two and three NH_3 molecules can be adsorbed per Fe site when gaseous NH_3 is introduced in Fe−BEA catalysts.[9] To study the influence of NH_3 on the decomposition of N_2O, two NH_3 molecules have thus been added to the previous models $[Fe-ON_2]^+$ and $Fe-BEA-ON_2$ (Figure 1c).

The electronic properties of these compounds are displayed in Table 4, whereas the approximate decomposition paths are presented in Figure 5 for $[Fe(NH_3)_2-ON_2]^+$ and in Figure 6 for $N_2O-Fe(NH_3)_2-BEA$.

Ammonia molecules are electron donating ligands, which essentially transfer their charge to Fe in the $[Fe(NH_3)_2-ON_2]^+$ model, leading to the distribution of the positive charge between the metal and the NH_3 molecules, although there is no spin delocalization on the ammonia ligands. The picture of the charge distribution is different in the presence of the BEA cluster. Indeed, as already reported for other TMI-zeolite models, the electronic charge from the NH_3 molecules is mainly transferred to the zeolite cluster.[54]

The formation energies, from the constituents, of the two initial complexes including 2 NH_3 ligands (Figures 5,6) are much larger than those without NH_3 (Figures 3,4), especially for $[Fe(NH_3)_2-ON_2]^+$. However, this is mainly due to the strong binding of NH_3 with Fe^+, and Fe−BEA to a lesser extent. Indeed, if the formation energy of $[Fe(NH_3)_2-ON_2]^+$ from Fe^+, $2NH_3$ and N_2O amounts to more than 80 kcal mol^{-1}, the binding energy of N_2O to $[Fe(NH_3)_2]^+$ is only 5.4 kcal mol^{-1}. Such a weak interaction explains the quite long $Fe-ON_2$ bond (2.32 Å) found for this complex.

In the same line, the stabilization of the products with respect to the initial complexes is also larger than for the associated compounds without ammonia.

The search for a maximum of the approximate decomposition path, related to the O−N bond elongation, leads to a species 15.0 kcal mol^{-1} higher in energy than the minimum $[Fe(NH_3)_2-ON_2]^+$ structure, and 30.2 kcal mol^{-1} higher than the stable $N_2O-Fe(NH_3)_2-BEA$ model.

The O−N bond lengths corresponding to the species at the maximum of the decomposition paths (Figures 5,6) are within 1.45−1.50 Å, whereas the Fe−O bond distances are decreased with respect to the initial complexes. The related $Fe-ON_2$ and $O-N_2$ BOs follow the same trends as previously mentioned for the models without NH_3, i.e., substantial increase and decrease, respectively. Finally, it is worth noting that these species include ON_2 groups which contain more electronic charge than their counterparts without NH_3, this charge originating essentially from Fe in $[Fe(NH_3)_2-ON_2]^+$, whereas all constituents, i.e., BEA, Fe and NH_3 participate in this donation in the case of $N_2O-Fe(NH_3)_2-BEA$.

Despite the lack of experimental data concerning the activation energy for N_2O dissociation in the presence of ammonia, it is of interest to evaluate the activation barrier from the reactants, $BEA-Fe + N_2O + 2NH_3$, to the approximate transition state, $BEA-Fe(NH_3)_2-O-N_2$. The calculated value of E_a at 500 K, using the activated complex theory, is 15.3 kcal mol^{-1}, i.e., 30% lower than without ammonia, showing that, already in the first step of Fe^{II} oxidation by N_2O, the presence of ammonia is energetically beneficial.

Again, modeling the Fe−zeolite with a single iron cation leads to a wrong description of the catalytic process, since there is no calculated activation barrier.

4.3. N_2O Dissociation. As shown from the results presented above, the dissociation mechanism involves both the $O-N_2$ bond elongation and the $Fe-ON_2$ bond shrinking. These two effects are clearly correlated. A substantial elongation (0.2−0.3 Å) of the O−N bond, even in the isolated N_2O molecule, stabilizes strongly the virtual antibonding σ (σ^*) orbital and decreases the HOMO−LUMO gap (by 1.3 eV for 0.2 Å elongation in N_2O). As expected, this elongation corresponds to a decrease of the Mayer BO (1.7 to 0.7 for 0.2 Å elongation).

The same effect occurs for the species determined at the maximum of the energy paths. These structures contain more electronic charge localized in the ON_2 group than without O−N elongation, favoring contributions of the antibonding O−N orbitals to the occupied molecular orbitals of the complex and weakening thus the O−N bond.

The $O-N_2$ bond, approximately a double bond, costs energy to elongate. This energy cost is partially compensated by the reinforcement of the $Fe-ON_2$ bond. The balance between these two effects gives the measure of the activation barrier. Its value depends thus, primarily, on the aptitude of the Fe^+ cation, and also of its environment, to compensate partly the loss of energy due to the $O-N_2$ bond stretching. For all models, one can say that, when the $O-N_2$ bond is elongated further than 1.45−1.50 Å, the energy gained by the Fe−O bond strengthening is larger than the energy loss and the reaction leads to the final products where the Fe−O bond is shortened to 1.65−1.70 Å.

The basic mechanism of N_2O dissociation is similar for an isolated Fe^+ cation and a neutral model of Fe(II)-zeolite. However, for a valid quantitative description of the chemisorption energies and activation barriers, it is quite necessary to include the zeolite framework in the model.

5. Conclusions

This study allows us to draw two main conclusions, the first more theoretical and the second more mechanistic.

The results obtained with Fe^+ or $Fe(NH_3)_2^+$ are not comparable with those obtained using Fe−BEA and Fe−BEA$(NH_3)_2$. The energetic is different: both original complex and products (in eq 1, section 3) are less stable when the BEA cluster is involved and the activation barrier is significantly higher, in good agreement with the experimental data. Moreover, the electron distribution in the complexes containing N_2O and both N_2O and NH_3 is different for Fe^+ and Fe−BEA. These differences show the decisive role played by the zeolite, able to take or release charge when ligands adsorb or desorb. This aptitude to regulate the charge distribution is certainly a decisive asset for catalysis by TMI-zeolites.

The role of NH_3 in the selective catalytic reduction is not restricted to the reduction step, as proposed generally, the presence of one or two ammonia molecules allows to reduce the activation barrier to N_2O dissociation on Fe^{II}. The calculated binding energies of Fe−O in BEA−FeO (93 kcal mol^{-1}) and BEA−Fe$(NH_3)_2$O (68 kcal mol^{-1}) show that the presence of adsorbed NH_3 makes also the abstraction of the oxygen easier. According to our results, the presence of ammonia is thus efficient in both steps of SCR, favoring energetically both the dissociation of N_2O, to yield "$Fe^{III}O$", and the removal of the so-called α-oxygen, leading back to the Fe(II) species.

Acknowledgment. This work has been performed in the framework of a Mexican-French PCP-CONACYT collaboration (PCP#00/01). Mrs. Sara Jiménez Cortés is acknowledged for her work with the references.

References and Notes

(1) Kuhn, G.; Schumacher, V.; Wagner, E. *Proceeding of the International Fertiliser Society Meeting*; London, 1999, The International Fertiliser Society, p 2.

(2) Suzuki, E.; Nakashiro, K.; Ono, Y. *Chem. Lett*. **1988**, 953. Gubelmann, M.; Tirel, P.-J. *Fr. Patent* 2.630.735, 1988. Kharitonov, A. S.; Alexandrova, T. N., Vostrikova, L. A.; Ione, K. G.; Panov, G. I. *Russ. Patent* 4.445.646, **1988**.

(3) Panov, G. I.; Uriarte, A. K.; Rodkin, M. A.; Sobolev, V. I. *Catal. Today* **1998**, *41*, 365.

(4) Panov, G. I.; Sobolev, V. I.; Dubkov, K. A.; Parmon, V. N.; Ovanesyan, N. S.; Shilov, A. E.; Shteiman, A. A. *React. Kinet. Catal. Lett.* **1997**, *61*, 251.

(5) Arbuznikov, A. V.; Zhidomirov, G. M. *Catal. Lett.* **1996**, *40*, 17.

(6) Lazar, K.; Lejeune, G.; Ahedi, R. K.; Shevade, S. S.; Kotasthane, A. N. *J. Phys. Chem. B.* **1998**, *102*, 4865.

(7) Yoshizawa, K.; Shiota, Y.; Yumuara, T.; Yamabe, T. *J. Phys. Chem. B.* **2000**, *104*, 734. Jia, J.; Pillai, S.; Sachtler, W. M. H. *J. Catal*. **2004**, *221*, 119.

(8) (a) Kögel, M.; Sandoval, V. H.; Schwieger, W.; Tissler, A.; Turek, T. *Catal Lett.* **1998**, *51*, 23. (b) Pophal, C.; Yogo, T.; Yamada, K.; Segawa, K. *Appl. Catal. B* **1998**, *16*, 177. (c) Centi, G.; Vazzana, F. *Catal. Today* **1999**, *53*, 683. (d) Kaptjein, F.; Marbán, G.; Rodríguez-Mirasol, J.; Moulijn, J. A. *J. Catal.* **1997**, *167*, 256. (e) Mauvezin, M.; Delahay, G.; Coq, B.; Kieger, S. *Appl. Catal. B.* **1999**, *23*, L79. (f) Coq, B.; Mauvezin, M.; Delahay, G.; Kieger, S. *J. Catal*. **2000**, *195*, 298. (g) Kameoka, S.; Takeda, T.; Tanaka, S.; Ito, S.; Yuzaki, K.; Miyadera, T.; Kunimori, K. *12th International Congress on Catalysis*, Granada, 2000, Recent Research Report n*o*. 30 (on CD rom)

(9) Mauvezin, M.; Delahay, G.; Coq, B.; Kieger, S.; Jumas, J. C.; Olivier-Fourcade, J. *J. Phys. Chem. B* **2001**, *105*, 928.

(10) Yakovlev, A. L.; Zhidomirov, G. M.; Van Santen, R. A. *Catal. Lett.* **2001**, *75*, 45.

(11) Yakovlev, A. L.; Zhidomirov, G. M.; Van Santen, R. A. *J. Phys. Chem. B* **2001**, *105*, 12 297.

(12) Ryder, J. A.; Chakraborty, A. K.; Bell, A. T. *J. Phys. Chem. B* **2002**, *106*, 7059.

(13) Higgins, J. B.; Lapierre, R. B.; Schlenker, J. L.; Rohrman, A. C.; Wood, J. D.; Kerr, G. T.; Rohrbaugh, W. J. *Zeolites* **1988**, *8*, 446.

(14) Löwenstein, W. *Am. Miner.* **1954**, *39*, 92.

(15) *Cerius2: Molecular Modeling Software for Materials Research*; Biosym Technologies/Accelerys: San Diego, CA, 1993.

(16) Berthomieu, D.; Ducéré, J. M.; Goursot, A. *J. Phys. Chem. B* **2002**, *106*, 7483.

(17) Yakovlev, A. L.; Zhidomirov, G. M.; Van Santen, R. A. *Catal. Lett.* **2000**, *70*, 175.

(18) Groothaert, M. H.; Schoonheydt, R. A.; Delabie, A.; Pierloot, K. *Catalysis by Unique Metal Ion Structures in Solid Matrixes*; Kluwer: Doordrecht Netherlands, 2001, Vol. 13, pp 205−220.

(19) Berthomieu, D.; Krishnamurty, S.; Coq, B.; Delahay, G.; Goursot, A. *J. Phys. Chem. B*, **2001**, *105*, 1149.

(20) Berthomieu, D.; Goursot, A.; Ducéré, J. M.; Delahay, G.; Coq, B.; Martinez, A. *Stud. Surf. Sci. Catal.* **2001**, *135*, 15-P151.

(21) Casida, M. E.; Daul, C.; Goursot, A.; Koester, A.; Pettersson, L.; Proynov, E.; St-Amant, A.; Salahub, D. R.; Duarte, H.; Godbout, N.; Guan, J.; Jamorski, C.; Leboeuf, M.; Malkin, V.; Malkina, O.; Sim, F.; Vela, A. *deMon Software, deMonKS3 Module*, University of Montreal, Montreal: **1996**

(22) Köster, A. M.; Geudtner, G.; Goursot, A.; Heine, T.; Vela, A.; Salahub, D. R. deMon, Ottawa, Canada, **2001**.

(23) Frisch, M. J.; Trucks, G. W.; Schlegel, H. B.; Gill, P. M. W.; Johnson, B. G.; Robb, M. A.; Cheeseman, J. R.; Keith, T. A.; Petersson, G. A.; Montgomery, J. A.; Raghavachari, K.; Al-Laham, M. A.; Zakrzewski, V. G.; Ortiz, J. V.; Foresman, J. B.; Cioslowski, J.; Stefanov, B. B.; Nanayakkara, A.; Challacombe, M.; Peng, C. Y.; Ayala, P. Y.; Chen, W.; Wong, M. W.; Andres, J. L.; Replogle, E. S.; Gomperts, R.; Martin, R. L.; Fox, D. J.; Binkley, J. S.; Defrees, D. J.; Baker J.; Stewart, J. P. Head-Gordon, M.; González, C. and Pople, J. A. Gaussian 94, Revision D.4. Gaussian Inc., Pittsburgh, PA, 1995.

(24) Perdew, J. P.; Wang, Y. *Phys. Rev. B.* **1986**, *33*, 8800.

(25) (a) Perdew, J. P. *Phys. Rev. B.* **1986**, *33*, 8822. (b) Perdew, J. P. *Phys. Rev. B.* **1986**, *34*, 7406.

(26) Godbout, N.; Salahub, D. R.; Andzelm, J.; Wimmer, E. *Can. J. Phys.* **1992**, *70*, 560.

(27) Hay, P. J. *J. Chem. Phys*. **1977**, *66*, 4377.

(28) Wachters, A. J. H. *J. Chem. Phys*. **1970**, *52*, 1033−1036; Wachters, A. J. H. *IBM Technol. Rept.* **1969**, RJ584.

(29) Becke, A. D. *Phys. Rev. A.* **1988**, *38*, 3098.

(30) Kutzler, G.; Painter, G. *Phys. Rev. B* **1990**, *43*, 6865.

(31) Mineva, T.; Goursot A.; Daul, C. *Chem. Phys. Lett*. **2001**, *350*, 147.

(32) Becke, A. D. *J. Chem. Phys.* **2002**, *117*, 6935.

(33) Weinert, M.; Watson, R. E.; Fernando, G. W. *Phys. Rev. A*, **2002**, *66*, 32508.

(34) Condon, E. U.; Shortley, G. H. In *The Theory of Atomic Spectra*; Cambridge University Press: New York, 1959, p 190.

(35) Baerends, E. J.; Branchadell, V.; Sodupe, M. *Chem. Phys. Lett*. **1996**, *265*, 481.

(36) Mineva, T.; Goursot A., to be published.

(37) Schafer, A.; Hora, H.; Ahlrichs, R. J. *Chem. Phys.* **1992**, *97*, 2571.

(38) Bauschlicher, C. W., Jr. *Theor. Chim. Acta* **1995**, *92*, 183.

(39) Moore, C. E. *Atomic Energy Levels. As Derived from the Analyses of Optical Spectra*; United States Department of Commerce. National Bureau of Standards: Washington, D. C. 1949.

(40) Delahay, G.; Berthomieu, D.; Goursot, A.; Coq, B. *Interfacial Application in Environmental Engineering and Catalysis*; Keane, M. A., Ed., Surfactant Science Series 108, Marcel Dekker: 2003, p 1.

(41) Trout, B. L.; Chakraborty, A. K.; Bell, A. T. *J. Phys. Chem.* **1996**, *100*, 17582.

(42) Laidler, K. J.; Glasstone, S.; Eyring, H. *J. Chem. Phys*. **1940**, *8*, 659; Laidler, K. J.; Glasstone, S.; Eyring, H. *J. Chem. Phys.* **1940**, *8*, 667.

(43) Germain, J. E. In *Catalyse Hétérogène*; Dunod: Paris, 1959, p 207.

(44) Atkins, P. W. in *Physical Chemistry*, Oxford University Press: New York, 1998, p 830.

(45) Haw, J. F.; Hall, M. B.; Alvarado-Swaisgood, A. E.; Munson, E. J.; Lin, Z.; Beck, L. W.; Howard, T. *J. Am. Chem. Soc*. **1994**, *116*, 7308.

(46) Kachurovskaya, N. A.; Zhidomirov, G. M.; Hensen, E. J. M.; van Santen, R. A. *Catal. Lett*. **2003**, *86*, 25.

(47) Mayer, I. *Int. J. Quantum Chem*. **1984**, *26*, 151.

(48) Wesolowski, T. A.; Goursot, A.; Weber, J. *J. Chem. Phys*. **2001**, *115*, 4791.

(49) Delabie, A.; Vinckier, C.; Flock, M.; Pierloot, K. *J. Phys. Chem. A* **2001**, *105*, 5479.

(50) Yoshizawa, K.; Yumura, T.; Shiota, Y/; Yamabe, T. *Bull. Chem. Soc. Jpn*. **2000**, *73*, 29.

(51) Delabie, A.; Pierloot, K. *J. Phys. Chem. A* **2002**, *106*, 5679.

(52) Delahay, G.; Mauvezin, M.; Guzman-Vargas, A.; Coq, B. *Catal. Commun.* **2002**, *3*, 385.

(53) The enthalpy of adsorption on N_2O on a 1.9 wt %Fe−BEA catalyst has been determined at 300 ± 0.01 K using a flowing microcalorimeter (SETARAM TG-DSC-111), with N_2O/He (2/98); the catalyst was first prereduced at 773 K with H_2/Ar (3/97)

(54) Goursot, A.; Coq, B.; Fajula, F. *J. Catal*. **2003**, *216*, 324.